Available online at www.sciencedirect.com

SCIENCE DIRECT®

Remote Sensing of Environment 93 (2004) 311–327

Remote Sensing of Environment

www.elsevier.com/locate/rse

Automated detection of thermal features of active volcanoes by means of infrared AVHRR records

Nicola Pergola[a,*], Francesco Marchese[b], Valerio Tramutoli[c,d]

[a]National Research Council, Institute of Methodologies of Environmental Analysis, C. da S. Loja, Tito Scalo, Potenza 85050, Italy
[b]University of Basilicata, Department of Geological Sciences Campus di Macchia Romana Potenza Italy
[c]University of Basilicata, Department of Engineering and Physics of the Environment Campus di Macchia Romana Potenza Italy
[d]National Research Council, Institute of Metodologie of Environmental Analysis Tito Scalo (PZ) Italy

Received 12 February 2004; received in revised form 16 July 2004; accepted 16 July 2004

Abstract

An innovative, Advanced Very High Resolution Radiometer (AVHRR)-based technique for improved automatic detection of volcanic hotspots and thermal anomalies is proposed in this paper. It is mainly based on a multitemporal analysis of historical, long-term satellite records. Such a technique basically rests on the Robust AVHRR Techniques (RAT) approach, which has been already successfully applied to several natural and environmental emergencies (e.g., fires, floods, earthquakes). In this work, the proposed technique has been tested on an extended set of eruptive events of Mt. Etna and Stromboli volcanoes. Results achieved, in terms of reliability (low false alarm rate) as well as of effectiveness (detection sensitivity), are described in detail. Moreover, the potential in low-level thermal anomaly detection, as possible pre-eruptive thermal signs, is also addressed and preliminary results obtained for a couple of events, discussed. The study cases here presented show the benefits of such a technique especially when different observational conditions (time/season of pass, atmospheric moisture content, solar illumination, satellite angles of view, etc.) are considered, making such a method globally applicable.

The future prospects, also in terms of possible operational scenarios, coming from the implementation of such an approach on the new generation of satellite sensors (such as SEVIRI aboard Meteosat Second Generation) are also discussed.

Keywords: Thermal features; Active volcano; Infrared AVHRR

1. Introduction

Volcanoes represent a serious potential danger for both the environment and population. In earlier times, volcanic eruptions have often caused great loss of lives and damage to the surrounding environment. Even today, when new scientific and technological findings have been reached, volcanoes remain dangerous, stimulating scientists to increasingly improve their capabilities of observing, monitoring and interpreting signs of volcanic unrest.

Since 1964, when the Nimbus-1 satellite was used to detect hotspots on Manua Loa and Kilauea volcanoes (Gawarecki et al., 1965), several satellite platforms have been used to study volcanic thermal activity. Sensors like the Thematic Mapper (TM) aboard the Landsat satellite series, have been extensively used to detect hotspots, thanks to their high spatial resolution (Gaonac'h & Vandemeulebrouck, 1994; Rothery et al., 1988). Nevertheless, low observational frequency (16 days in between two consecutive passes, without clouds hiding the target area) and high cost of images have rendered them ineffective for real-time monitoring and operational purposes (Carn & Oppenheimer, 2000).

The Advanced Very High Resolution Radiometer (AVHRR) aboard NOAA satellites, with an observational frequency of 6 h, was one of the first instruments widely used (and still nowadays) for near real-time volcano activity monitoring, in terms of ash cloud detection and tracking (e.g., Pergola et al., 2004; Prata, 1989, Schneider & Rose,

* Corresponding author. Tel.: +39 971 427268; fax: +39 971 427271.
E-mail address: pergola@imaa.cnr.it (N. Pergola).

0034-4257/$ - see front matter © 2004 Elsevier Inc. All rights reserved.
doi:10.1016/j.rse.2004.07.010

1994; Schneider et al., 1995) as well as in terms of thermal features recognition (e.g., Harris et al., 1995b,a).

The spectral radiance emitted by hot volcanic sources like molten lava or high temperature gas emissions, reaches its maximum in the region of midinfrared (MIR, around 3 μm). Consequently, AVHRR channel 3 (3.5–3.9 μm), has been widely used for lava flow monitoring, despite its relatively coarse ground resolution cell (1.1-km nadir view). In fact, as demonstrated by Dozier (1981), the presence of a high temperature source, even affecting only a small portion of one AVHRR pixel, causes a dramatic increase of the emitted MIR radiance as well. Moreover, the high sampling frequency of AVHRR (4 passes per day, at least) makes this instrument ideal for near real-time monitoring of dynamic volcanic systems.

However, in spite of these advantages, some problems arise when automatic and reliable procedures for hotspot detection have to be designed and implemented. Major difficulties have been identified in choosing appropriate thresholds suitable to discriminate between actual and false volcanic hotspot identifications. For example in daytime, in the 3–5 μm window, the reflected component of solar radiation and the natural warming of volcanic rocks (because of solar heating) may both produce high thermal radiation in AVHRR channel 3 and possibly generate false hotspot identifications (Di Bello et al., in press; Harris et al., 1995b,a; Oppenheimer, 1998; Wright et al., 2002). To face such a problem, which becomes much more serious as far as an operational scenario is aimed at, Harris et al. (1995a) proposed a differential approach based on the spectral comparison between two brightness temperatures measured in AVHRR channel 3 and channel 4 (10.3–11.3 μm). Since channel 3 is more sensitive than channel 4 to the hot sources at magmatic temperatures and both should be equally sensitive to solar heated surfaces, volcanic hotspots are expected to exhibit higher $\Delta T=(T_3-T_4)$ values. For this reason, Harris et al. (1995a) suggested a fixed threshold test, $\Delta T>10$ K, to identify volcanic hotspots by AVHRR observations. Nonetheless, this methodology is not always reliable, mainly because it is based on a fixed threshold used under whatever observational and environmental conditions. In fact, as already observed by other authors (e.g., Harris et al., 2001; Higgins & Harris, 1997), high brightness temperature differences between AVHRR channels 3 and 4, can also be observed because of atmospheric effects, differential emissivity and/or contribution of reflected radiation to the MIR signal. Therefore, $\Delta T=T_3-T_4$ can be greater than 10 K even if there are no active volcanic surfaces.

A similar approach was used by Higgins and Harris (1997) to detect thermal anomalies on Mount Etna, Stromboli and Vulcano. Afterwards it was implemented on GOES-IMAGER sensors, improving its capabilities by using two different thresholds, one to be used for daytime data and another for nighttime records (Harris et al., 1999). However, as stated before, the differential method may generate false alarms also because of the clouds which absorb the thermal radiation emitted by the Earth's surface more in the spectral band of channel 4 than the one of channel 3, so that $\Delta T>10$ K owing to very low values of T_4 (Di Bello et al., in press; Harris et al., 2001; Marchese, 2001). Furthermore, for a specific class of meteorological clouds (e.g., cumulus), this brightness temperature difference ΔT can assume high positive values because of emissivity. In fact, the radiation measured in AVHRR band 3 is generally upwelling from lower levels of clouds, where temperatures are warmer whereas, on the other side, the radiation measured in channel 4 typically originates from the cloud top (colder) layers.

Because of the high variability of volcanism and environmental conditions, the use of long-term remotely sensed thermal data has also been proposed lately (Dean et al., 1998; Dehn et al., 2000). Such authors suggest the use of temporal satellite series to monitor fluctuations in radiant temperatures over volcanically active areas. These studies suggesting for the first time dynamic, rather than fixed thresholds, represent a clear improvement for automated detection purposes.

A near real-time hotspot monitoring system was proposed afterwards by Harris et al. (2001). This method, based on brightness temperature differences as well, between channel 2 (at 3.9 μm) and channel 4 (at 10.4 μm) of GOES ($\Delta T=T_2-T_4$), scans a pixel target area centred on predefined volcano coordinates searching for anomalous ΔT. The standard variation σ and the mean of ΔT, are calculated for a 5-pixel band around the target box, and pixels with $\Delta T>3.3\sigma$ above the mean are flagged as hot. The values of the mean and standard variation are then recalculated until no new hot pixels are flagged. This method represents, in terms of false alerts, an improvement compared to the previous techniques, even if false identifications (related to high cloud reflectance that can produce high ΔT values) and no-detection cases still remain, as reported by the authors themselves (Harris et al., 2001).

Recently, Harris et al. (2002) have proposed an improved algorithm to detect hotspots based on a probability test. This method has been used to detect hotspots on Kilauea volcano by means of GOES data but it can also be applied to AVHRR records. It improves the detection of hotspots but, as explained by authors themselves, it still causes false alarms owing to cosmic hits and cloud edge effects. Finally, except for a recently proposed algorithm which uses MODIS data (Flynn et al., 2002; Wright et al., 2002, 2004) and which is, however, limited to nighttime observations, no other techniques, among the ones proposed for automatic hotspot detection, can be reliably applied at the global scale and in whatever observational conditions.

If real-time (or near real-time) monitoring is aimed at, targeted to volcanic hazard mitigation purposes, timely and reliable detections are required. Frequent observations and effective satellite products should be made available on a global scale to assure an actual operational surveillance

system. This suggests the development of new satellite techniques, providing reliable and effective products, with an adequate sampling, able to perform consistently under different environmental and observational conditions.

In this paper, a new strategy of satellite data analysis, the so-called Robust AVHRR Techniques (RAT) approach (Tramutoli, 1998), already applied to several natural and environmental emergencies (e.g., Cuomo et al., 2001; Pergola et al., 2001; Pergola & Tramutoli, 2003; Tramutoli et al., 2001a, 2001b), is proposed for automated detection of volcanic thermal features on a global scale and in any observational conditions. It has been applied to several eruptive events recently occurred at Mt. Etna and Stromboli volcanoes, to evaluate its reliability in terms of detection sensitivity as well as in terms of false alarm reduction. Different eruptive events, occurring in day and nighttime and during Winter and Summer seasons, have been considered in order to assess method performances and possible limitations under different observational conditions. The potential of the proposed technique in detecting possible pre-eruptive thermal anomalies has also been addressed and results presented for a couple of Mt. Etna eruptive events.

2. A new approach for automatic detection of volcanic thermal activity: the RAT method

Automatic methods for volcanic hotspot detection by satellite have to deal with the problem of identifying thresholds which, at global scale and in any observational and environmental conditions, should be able to distinguish between pixels actually representing volcanic hotspots and pixels that do not. A reliable and effective discrimination can be hard to achieve due to the high intrinsic variability that a satellite signal may normally have.

Generally speaking, a signal measured by a satellite-borne sensor shows a sort of natural intrinsic variability mainly due to the fluctuations that several related parameters (e.g., atmosphere and surface properties) naturally undergo, depending on the specific observational, geographical and environmental conditions (hour of pass, geographic latitude, season, angle of view, sun/satellite relative position, etc.). This type of "natural/observational noise" typically generates spurious effects producing non-negligible perturbations on the signal, especially when an analysis in the space–time domain has to be carried out. A new approach called Robust AVHRR Techniques (RAT), first proposed by Tramutoli (1998) suggests the possibility of using long-term multitemporal satellite records in order to characterise the signal under investigation and to generate dynamic, variable and *llocal* (i.e., local in space and time domain) thresholds which, by construction, result less affected by the above mentioned observational/natural noise. Such an approach has already been tested on the monitoring of different natural hazards, like earthquakes (Di Bello et al., in press; Tramutoli et al., 2001a) and floods (Lacava et al., in press). Concerning volcanic activity, RAT has already been applied for ash cloud detection/discrimination purposes (Di Bello et al., in press; Pergola et al., 2001, 1998, 2004), as well as to stratospheric volcanic cloud monitoring (Tramutoli et al., 2001b). Regarding its applicability to hotspot detection, an extended study has already been carried out for forest fire detection with very promising results (Cuomo et al., 2001; Lasaponara et al., 1998). In this study, the RAT approach is applied, for the first time, to an extended set of eruptive events, giving a first assessment of its potential contribution to the implementation of an automatic, global system for volcanic hotspot detection and, possibly, for an early identification of pre-eruptive thermal anomalies.

2.1. The approach rationale

The RAT method considers every thermal anomaly in the space–time domain as a deviation from a normal state which should be preliminarily defined. Readers can find a detailed description of the theoretical background of such an approach as well as an extended set of its possible applications in Cuomo et al. (2001), Di Bello et al. (in press), Pergola et al., (2001, 2004), Tramutoli (1998) and Tramutoli et al. (2001a). In the following, only a quick reminder of the approach rationale will be given.

Considering a collection of multitemporal, colocated imagery as a space–time process, described at each place (x,y) and time t, by the *llocal* (i.e., in space and time domains) value of the satellite derived measurements $V(x,y,t)$, the RAT implementation can be done by computing for each homogeneous (i.e., collected at the same time of day, month of year, under similar observational conditions) imagery data set an expected value of the signal, $V_{\mathrm{REF}}(x,y)$ and its natural variability, $\sigma_{\mathrm{V}}(x,y)$, due to all the possible noise sources which are not related with the event to be monitored. Afterwards, a change detection step is computed by calculating a local index of change, the so-called Absolutely Llocal Index of Change of the Environment (ALICE) $\otimes_{\mathrm{V}}(x,y,t)$ which provides, at the pixel level, an estimate of how much the signal under investigation $V(x,y,t)$, (i.e., observed at time t) differs from its "normal" behaviour in unperturbed conditions, $V_{\mathrm{REF}}(x,y)$ and how much such a deviation is statistically significant with respect to the natural variability, $\sigma_{\mathrm{V}}(x,y)$. The mathematical definition of this index is:

$$\otimes_{\mathrm{V}}(x,y,t) \equiv \frac{V(x,y,t) - V_{\mathrm{REF}}(x,y)}{\sigma_{\mathrm{V}}(x,y)} \quad (1)$$

where $V(x,y,t)$ is the signal measured by satellite at location (x,y) at time t, $V_{\mathrm{REF}}(x,y)$ and $\sigma_{\mathrm{V}}(x,y)$ are the reference fields, computed for the same location on time series of colocated, homogeneous (for time slot, month of year, etc.) satellite images. The robustness of this approach is intrinsic because higher signal variability $\sigma_{\mathrm{V}}(x,y)$ (in the chosen

spatial/temporal domain) will result in lower values of $\otimes_V(x,y,t)$, reducing, in this way, the problem of false alarms.

Concerning its application to hotspot detection, the RAT approach has been implemented as a three-step process:

(1) Data preprocessing (collection, radiometric calibration and precise navigation)
(2) Construction of reference fields
(3) Automatic Hotspot and Thermal anomaly Detection.

2.2. Data preprocessing (collection, radiometric calibration and precise navigation)

In order to produce homogenous data sets, first of all NOAA-AVHRR data acquired throughout a 6-year span (1995–2001) were put together, stratified according to the month of acquisition and to the hour of pass. Subscenes, 1024×1024 sized covering the whole Italian peninsula, part of Dalmatian coasts of Croatia and southern coasts of France (see Fig. 1) have been extracted and used in the space–time processing step.

Six months (January, February, July, September, October and November) and three "temporal windows" (00:00–02:00GMT i.e., local night, 12:00–15:00GMT, i.e., local day, 17:00–19:00GMT, i.e., local afternoon) were chosen according to the eruption occurrences and in order to test RAT performances under different observational and natural conditions.

At the end of this step, 18 different data sets were defined (three temporal windows for each one of the 6 months), each one accommodating homogeneous images, for a final total number of more than 800 AVHRR scenes to be processed.

The second step was the radiometric calibration (performed following standard calibration procedures like the one described in Kidwell, 1991) and the navigation and colocation, carried out by means of a precise, purposely developed scheme which is able to assure a final accuracy of one AVHRR pixel (Pergola & Tramutoli, 2000, 2003).

All data were put in the same geographic projection (Lambert Azimuthal Equal Area) and in this way, colocated in the space–time domain as shown in Fig. 1.

2.3. Construction of reference fields

Starting from the previous defined historical series of colocated satellite images, being $T_3(x,y)$ the brightness temperature measured in AVHRR channel 3, two reference fields were determined for each data set. The first one, $\langle T_3(x,y)\rangle$, represents the measure expected (i.e., arithmetic average in time domain) in unperturbed conditions at place (x,y). The second one, $\sigma_3(x,y)$, represents the normal variability of the signal (i.e., standard deviation in time domain), derived by the temporal analysis at the same place (x,y). Both reference fields have been computed by an automatic procedure, under homogeneous observational conditions, as described before. Moreover, a *k-σ clipping* filter (Tramutoli, 1998) was applied in order to automatically and iteratively remove from the historical data set possible outliers. Such extreme values could be

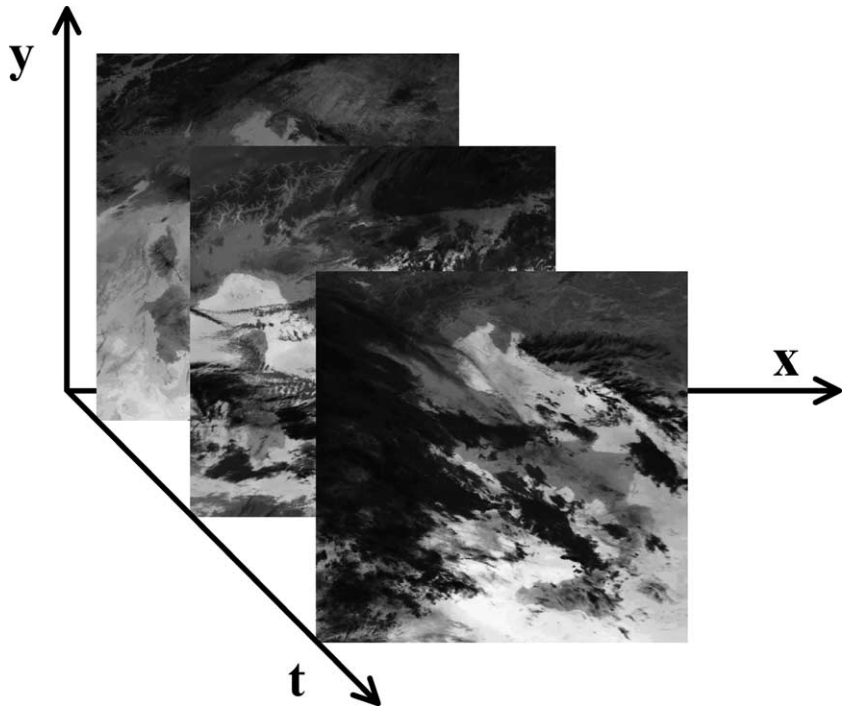

Fig. 1. Time series analysis of colocated subsets of AVHRR satellite imagery.

associated to clouds or to spurious effects that, although not related to the event under investigation, may alter the "normal state" of the signal and increase the natural noise level. The proposed filter flags as unusable all the individual pixels representing these extreme circumstances and excludes them for the next processing steps. In particular, by means of a previously derived land–sea/water mask, a 2σ-clipping filter was applied over land pixels and a 3σ-clipping filter over sea/water locations, given the lower natural variability of the signal on sea/water areas, than the one observed over land.

2.4. Automatic hotspot and thermal anomaly detection

In order to detect hotspots and to identify thermal anomalies the general ALICE index, defined in Eq. (1), has been adapted for this purpose and, consequently, computed as follows:

$$\otimes_3(x,y,t) = \frac{[T_3(x,y,t) - <T_3(x,y)>]}{\sigma_3(x,y)} \quad (2)$$

where $T_3(x,y,t)$ is the brightness temperature measured in AVHRR channel 3 at place (x,y) at time t, $<T_3(x,y)>$ and $\sigma_3(x,y)$ are, respectively, the temporal mean and the standard deviation in time domain, derived by the time-series analysis for the specific relevant period (1 month long) and for the selected temporal slot (night/day/afternoon), as described before. $\otimes_3(x,y,t)$ shows how much, in comparison with its historical "normal" variability, the signal at time t deviates from a reference value observed in unperturbed periods and in similar observational and natural conditions. The higher $\otimes_3(x,y,t)$ values are, the stronger are the related thermal anomalies and different levels of $\otimes_3(x,y,t)$ can be associated with different anomaly intensities (RAT tuneability). It should be stressed once more that the $\otimes_3(x,y,t)$ index, for construction, is expected to be significantly less affected by site effects. In fact, surface features (high reflective exposed soils, warmed volcanic rocks, etc.) are expected to show quite a similar behaviour during the same period of the year (month) and of the day (hour), so low values of $\otimes_3(x,y,t)$ are expected in these cases, even in the presence of high values of $T_3(x,y,t)$.

Moreover, this intrinsic RAT capability to eliminate/reduce site effects, allows the use of a single-channel approach (e.g., T_3), instead of a differential technique (e.g., T_3-T_4); this circumstance further reduces problems and limitations which are typical of the two-band methods (e.g., clouds, cloud edges, etc.).

In order to evaluate the performances of the proposed approach, $\otimes_3(x,y,t)$ index has been computed on AVHRR images collected during three recent eruptive events of Mt. Etna (January–February 1999, July–August 2001 and October–November 2002), and during the last Stromboli volcano eruptive activity of November–December 2002.

3. Application of RAT method to Etna and Stromboli eruptions

3.1. The January–February 1999 Mt. Etna eruption

Between September 1998 and January 1999, a series of 22 paroxysmal eruptive episodes occurred at SE Crater of Mt. Etna and the stronger strombolian event occurred on January, 23rd. These eruptions preceded the opening of a new fracture, on 4 February located on Southeast side of the SE Crater. This was the first lateral eruption occurred after the 1991–1993 eruptive events.

The new vent was very active producing plentiful lava flows, toward Valle del Bove until November 1999 (Behncke, 1999). The proposed RAT approach has been tested during this event, analysing all the AVHRR passes acquired in January and in February 1999.

3.1.1. Results

Some results of RAT application to the aforementioned event are reported in Fig. 2. In Fig. 2a, a magnification of the Etna area of the AVHRR pass acquired on 23 January 1999 at about 18 GMT (Local time=GMT+1) is reported in grey tones. On the same figure, thermally anomalous pixels detected by RAT, identified by $\otimes_3(x,y,t)>3$, are depicted in red. It appears clear that all the detected hotspots, as a result of the strong eruptive episode occurred on 23 January at SE Crater, are well located on the volcano edifice and in particular over the summit of the crater area where the activity was stronger. Similarly, hotspots detected by RAT on 6 February (Fig. 2b), 12 February (Fig. 2c) and 19 February (Fig. 2d) are all well related to the documented (Behncke, 1999) eruptive activity and, in particular, to the plentiful lava flows produced by the new fracture opened on 4 February on the volcano's flank. As can be seen, in spite of the different observational conditions (Fig. 2a and b is received in the afternoon, whereas Fig. 2c and d is acquired during the night), RAT was able to automatically detect hotspots without generating any false identification. Even if a large presence of meteorological clouds over the target area is observed (see, for instance, Fig. 2b and c), the proposed technique still saves its reliability and effectiveness as well as no false positive are identified in correspondence of those clouds.

3.2. The July–August 2001 Mt. Etna eruption

The Etna eruption in July 2001 originated from seven different fissure systems located on the south and northeast flanks of the volcano. Some of the flank activity was unusually violent with magmatic explosions and abundant emission of pyroclastics (Behncke, 2001). In the evening of July 4th, the 12th eruptive episode in 30 days occurred at the Southeast Crater, and a lava effusion from the Levantino cone formed two flows oriented toward NE and SSE. The 13th eruptive episode occurred on 7 July, with lava flows

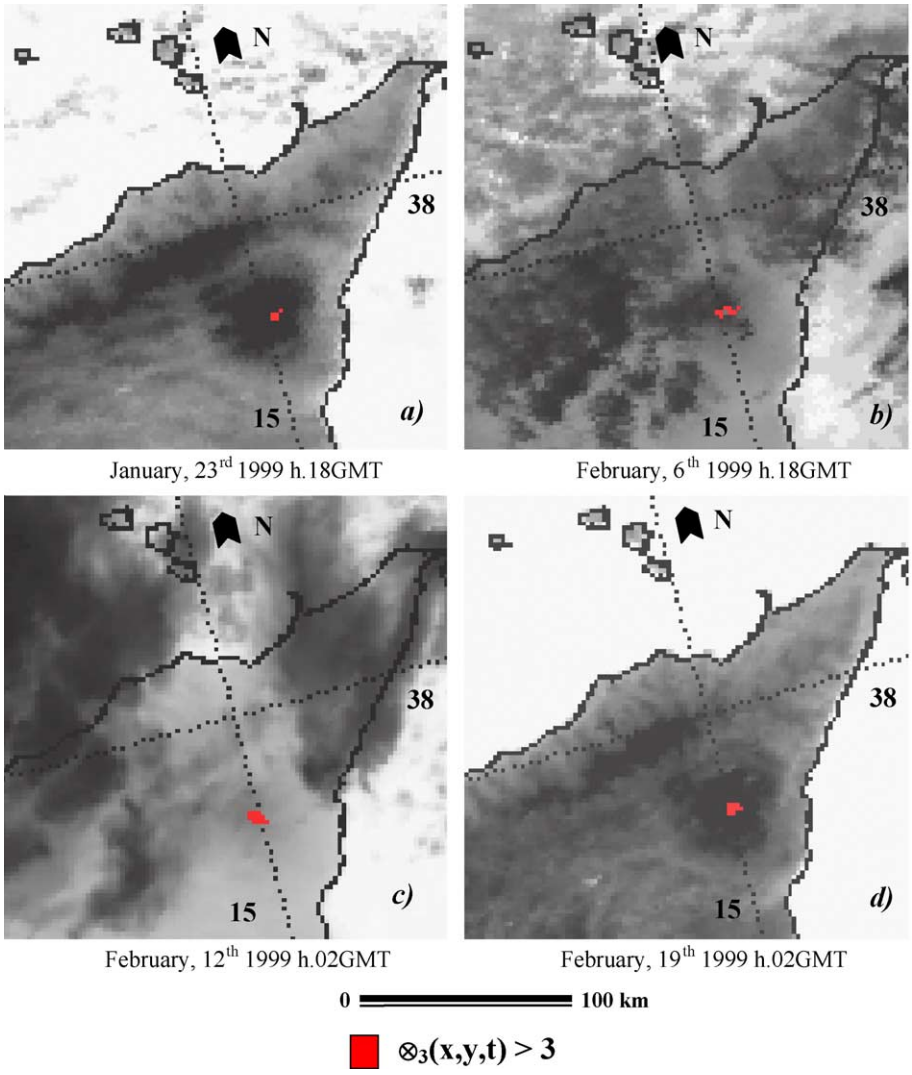

Fig. 2. RAT results obtained during the eruption of Mt. Etna occurred in January–February 1999 are shown. Background images are AVHRR thermal channels depicted in grey scale and magnified around Mt. Etna, where higher values of brightness temperature are reported in brighter tones. Coastlines are reported in black. Pixels identified as anomalous with $\otimes_3(x,y,t)>3$ are depicted in red. (a) 23 January 1999 18 GMT; (b) 6 February 1999 18 GMT; (c) 12 February 1999 02 GMT; (d) 19 February 1999 02 GMT.

from Levantino and powerful Strombolian explosions at the summit vent of SE Crater. After this event an intense paroxysmal event occurred on 13 July. This was followed by a long series of earthquake swarms with more than 2500 tremors (Behncke, 2001). On 17 July, the first fracture opened at the South base of the SE Crater, producing mild Strombolian activity, while a lava flow extended toward Belvedere. On the evening of the same day, another fracture opened at about 2700 m elevation, followed by the opening of new fractures on the flanks of the volcano during the following days.

The July–August 2001 eruption was very dangerous and it did cause damages to the cable car and ski lifts located between 1900 and 2600 m on the S flank of the volcano. The lava flow threatened the city of Nicolosi and artificial barriers were built in order to shield the Rifugio Sapienza's infrastructures. All the AVHRR passes acquired in July 2001 were analysed, in order to test performances of the RAT approach under very different conditions (high summer time) compared to the previous before described event which occurred in midwinter.

3.2.1. Results

In Fig. 3, some results obtained by analysing the AVHRR images acquired during this event are reported. Again, in order to test RAT technique in different observational conditions, daytime data as well as nighttime records were processed.

Two examples of nighttime results are shown in Fig. 3a (22 July 2001 at 01 GMT, Local Time=GMT+2) and in Fig. 3b (25 July 2001 at 00 GMT). The hotspots detected by RAT, red coloured in the figures, seem to properly describe the documented lava flows produced by the fractures opened on the flanks of the volcano as from 17 July. Once

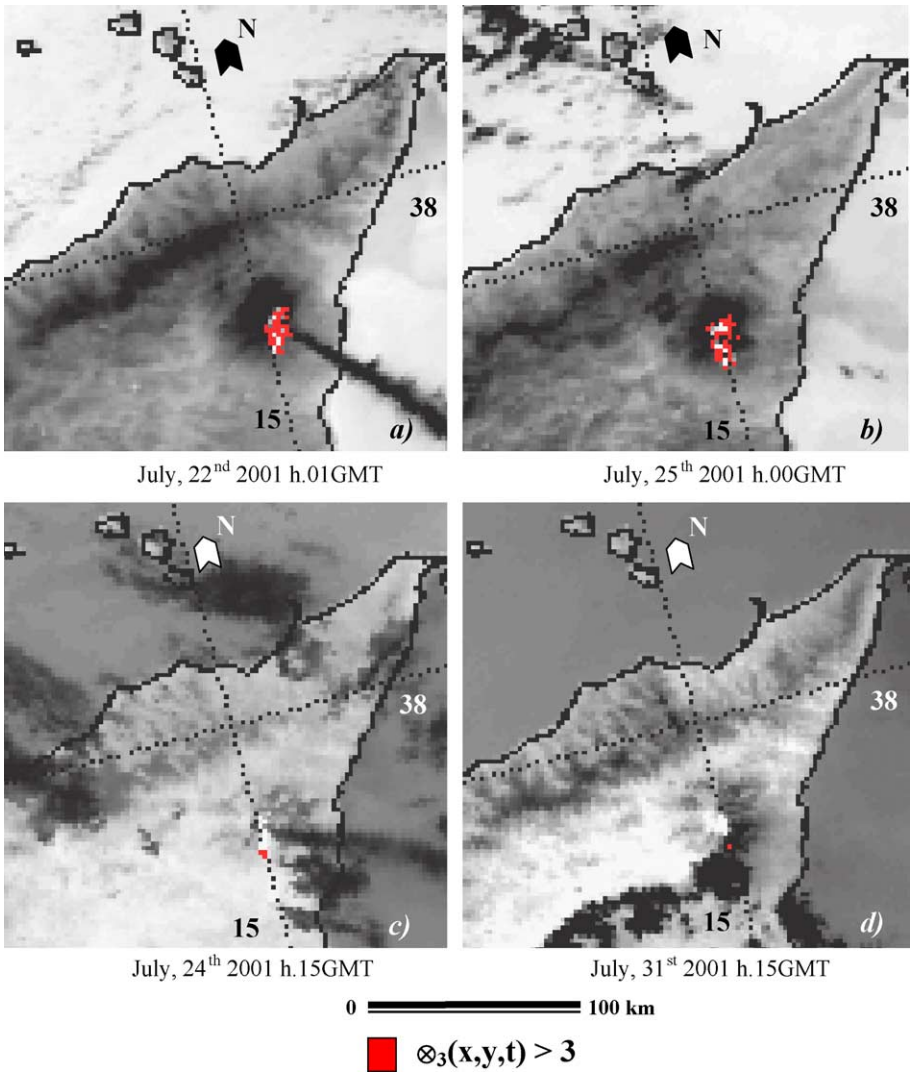

Fig. 3. RAT results obtained during the eruptions of Mt. Etna occurred in July–August 2001 are shown. Background images are magnifications around Mt. Etna of AVHRR thermal channels depicted in grey scale, where higher values of brightness temperature are reported in brighter tones. Coastlines are reported in black. Anomalies depicted in red represent pixels with $\otimes_3(x,y,t)>3$. (a) 22 July 2001 01 GMT; (b) 25 July 2001 00 GMT; (c) 24 July 2001 15 GMT; (d) 31 July 2001 15 GMT.

more, RAT automatically detected thermal anomalies without generating any false identification and with no need to define and identify different thresholds. Fig. 3 clearly highlight the self-adaptability of the proposed approach, which saved its reliability also in different natural and observational conditions.

Results obtained in daytime and reported in Fig. 3c (24 July at 15G MT) and Fig. 3d (31 July at 15 GMT), although showing a lower sensitivity of the proposed approach in daytime and in summer season, seem to provide a further confirmation of its above mentioned capability to avoid false alarms. In daytime, in fact, although the higher natural variability of the signal causes a weak degradation in RAT sensitivity, the ALICE index still remain not affected by reflected solar radiation and warming of volcanic rocks (effects which are both particularly significant in the selected observational conditions). In both cases, as shown in Fig. 3c and d thermal anomalies detected by RAT (red coloured) clearly underestimate the actual extension of the areas interested by the eruption but are still related to the actual paths of lava flows produced by the new fractures and once again, in spite of the very unfavourable observation conditions (high summer, in the middle of the day) no false alarms were generated. As stated before, the ALICE index offers the advantage to be tuned to the different environmental conditions; this opportunity could be exploited here in order to better describe size and extension of lava paths, even if a possible increasing in the false alarm rate should be taken into account. In fact, looking at Fig. 4, where three different ALICE cutting levels are used on images previously shown in Fig. 3c and d, it is clear that a better identification of the actual lava paths was achieved. However, it should be noted that a limited number of false positive thermally anomalous pixels were flagged, mainly

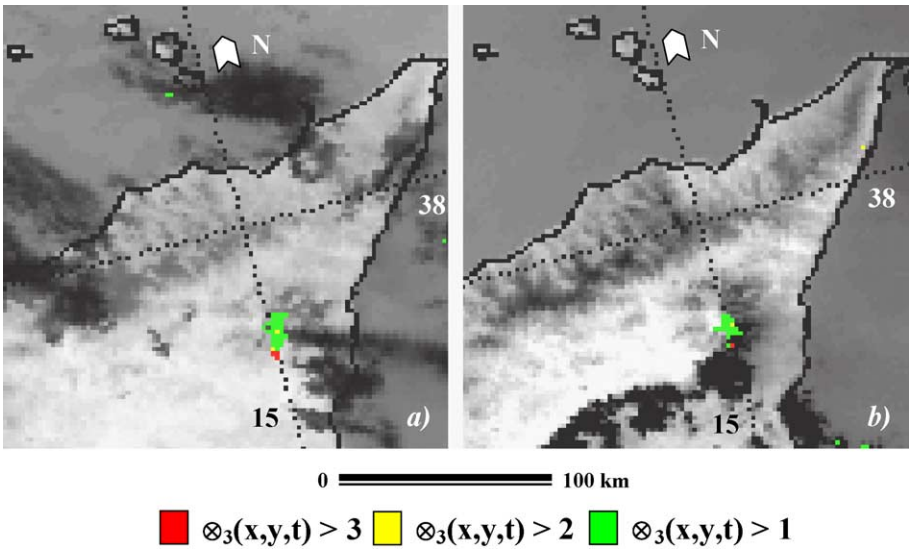

Fig. 4. (a) Like Fig. 3c (24 July 2001 15 GMT) and (b) like Fig. 3d (31 July 2001 15 GMT) but three cutting levels of ALICE index are shown here: red, yellow and green, respectively for pixels with $\otimes_3(x,y,t)>3$, $\otimes_3(x,y,t)>2$ and with $\otimes_3(x,y,t)>1$.

on part of clouds located over the sea. Therefore, thermal anomalies are better identified at lower values of ALICE index without, however, a significant reduction of RAT reliability (only few false detections occurred over the whole study area).

Thus, these results demonstrated the proposed approach is robust and tuneable and that it can be automatically applied under different observational conditions (day/night observations, Summer/Winter seasons, etc.) with a slight degradation in terms of sensitivity in critical (diurnal, high summertime records) observational conditions. Moreover, the way the ALICE index is constructed suggests the proposed approach is independent to geographic location and, for this reason, it is expected to be successfully applicable globally, on whatever volcano. Finally, the complete independence on the specific satellite platform, makes this approach applicable on whatever satellite system, allowing possible improvements in spectral, spatial and temporal resolutions.

3.3. The Mt. Etna and Stromboli events of October–November 2002

3.3.1. Etna eruption

The 2002 Etna flank eruption began on 27 October with the opening of two new fissures located one on the southern flank near Torre del Filosofo at about 2750 m elevation, and the other one on the northern flank of the volcano at about 2500 m, in an area known as the Northeast Rift (Behncke, 2002). During this event, different lava flows were emitted from the fissures, and significant ash plumes were produced. Lava flows from the northern fissure destroyed part of the ski lift in the area of Piano Provenzana, and they cut across the road connecting this area with the town of Linguaglossa. By 28 October, several portions of the pine forest were set ablaze, and several hotels, restaurants and power lines were destroyed by the lava flows (Behncke, 2002).

The lava flow from the southern fissure, started about 12 h after the northern one was split in two branches around Monte Nero, before it stopped on 31 October reaching a total length of 1 km.

A distinct decrease of the intensity of the volcanic activity was evident, from the third day of the eruption. On 5 November, lava flows from the northern fissure stopped and the first phase of eruption was considered ended (Smithsonian Institute, 2002).

A second phase of the eruption started on November 13th, with a new mild Strombolian activity and with new lava flows produced from the southern fissure opened on 26 October (Behncke, 2002).

3.3.2. Stromboli eruption

The eruption which occurred on 28 December was the first effusive eruption of Stromboli volcano after 17 years. The eruption started with a strong explosion that caused ash fallout on the village of Stromboli and the opening of a new fissure on the North East side of Crater 1. A lava flow came out from the fissure and three lava branches spreading within the Sciara del Fuoco reached the sea within 30 min. On 30 December, two landslides suddenly formed along Sciara del Fuoco and the contact with the sea formed two tsunamis with waves several meters high. The tsunamis damaged buildings and boats in the village of Stromboli and Ginostra (Smithsonian Institute, 2002). The Stromboli eruption of December 2002 was preceded by intense strombolian activity which started in May 2002. The maximum level was reached at the end of October and during the first 2 weeks of November, when an increase in the intensity of strombolian activity and more powerful eruptions with a larger number of ash eruptions occurred

(Smithsonian Institute, 2002). On November 19th, during a survey carried out by the Italian National Civil Protection Department using a thermal infrared camera from a helicopter, a very high level of the lava within the craters was observed (Smithsonian Institute, 2002). High levels of activity were also observed during the month of December before the beginning of the new flank eruption. The same AVHRR data sets were used for both Mt. Etna and Stromboli volcanoes to test RAT effectiveness in detecting thermally anomalous pixels during the aforementioned eruptive events.

3.3.3. Results

In Fig. 5a, a zoom around the Etna area of a nighttime image acquired on 29 October 2002 and processed by following RAT methodology is shown. As can be clearly seen, several thermal anomalies were detected on the Etna area. Two clusters of hotspots can be identified, in accordance with the actual distribution of lava flows produced by the two different fissures located on the northern and on the southern flanks of the volcano. A thermal anomaly was also detected on Stromboli volcano, where the high value of the $\otimes_3(x,y,t)$ index is properly related to the exceptional strombolian activity which occurred at the summit craters from the end of October. In Fig. 5b, another AVHRR pass recorded on 7 November 2002 is shown. Looking at the picture, it is evident that only few pixels were detected on the area of Etna volcano, according to the actual decreasing of volcanic activity. Once more, the spatial distribution of detected hotspots is rightly correlated with the actual location of lava flows, on the north as well as on the southern part of Etna. Once more, a thermal anomaly was detected on the area of Stromboli volcano as expected due to the observed, very intense strombolian activity which occurred that day. In Fig. 5c, a magnification of the AVHRR scene received on 20 November 2002 is shown. The comparison with the results obtained for the image of 29 October (Fig. 5a), shows that in this case, according to the documented eruption evolution, no hotspots were detected by RAT on the north side of Etna

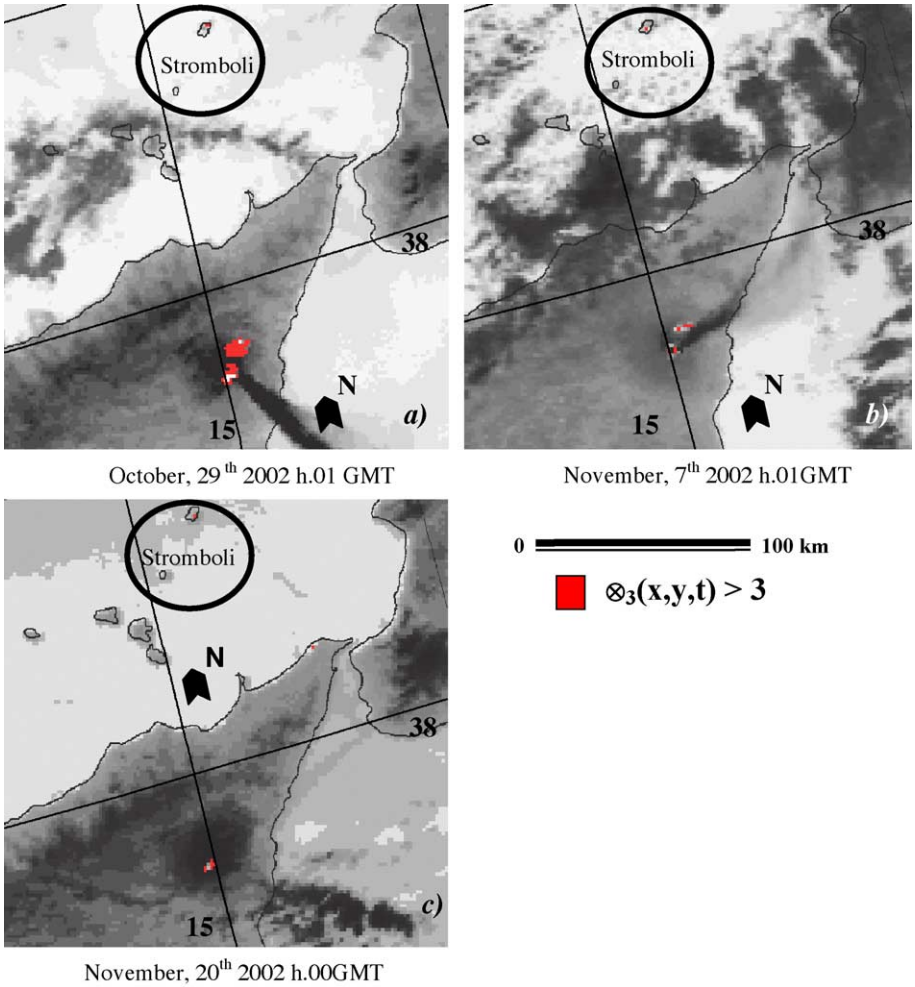

Fig. 5. RAT results obtained during the activity of Mount Etna and Stromboli volcanoes occurred in October–November 2002 are shown. Background images are magnifications around Mt. Etna of AVHRR thermal channels depicted in grey scale where higher values of brightness temperature are reported in brighter tones. Coastlines are reported in black. Pixels identified as anomalous with $\otimes_3(x,y,t)>3$ are depicted in red. (a) 29 October 2002 01 GMT; (b) 7 November 2002 01 GMT; (c) 20 November 2002 00 GMT. The Stromboli island is indicated by a black circle.

volcano. Hotspots detected on the south side of Etna are related to the second phase of the eruption started on 13 November. In this phase, only the southern fissure produced lava which continued to flow with some variations until 28 January 2003. Looking at the same figure, once again a clear thermal anomaly over Stromboli has been observed. Such an anomalous signal was independently confirmed by a helicopter survey carried out by the Italian National Civil Protection Department on 19 November, which reported an exceptional raising level of the magma within the craters (Ingv-Sezione di Catania, 2002). This phase was considered the prelude of the new flank activity, officially started on 28 December, which produced a considerable amount of lava and caused, a few days later, the collapse of more than 10 million cubic meters of volcanic rocks into the Mediterranean. It should be stressed again that, for all three images reported in Fig. 5, no false identifications have been produced by the proposed technique, neither in correspondence to meteorological clouds, nor from the volcanic plume, although both features were clearly present over the study area.

3.4. Precision assessment of thermal anomalies mapping

The study of the space–time evolution of the eruptive events of Etna and Stromboli volcanoes presented in this paper confirmed that RAT technique was able to correctly identify hotspots related to the actual volcanic activity, strongly reducing the problem of false identification.

In order to evaluate the precision (in the spatial domain) of the proposed approach in localising hotspots as well as its accuracy (in the temporal domain) in following the temporal evolution of activity (i.e., in terms of fluctuations of anomalies intensity), AVHRR data were colocated to a georeferenced map of the Etna area. In this way, it was possible to better evaluate whether thermal anomalies detected by RAT were spatially related to the actual paths of the lava flows produced during the eruptions and in

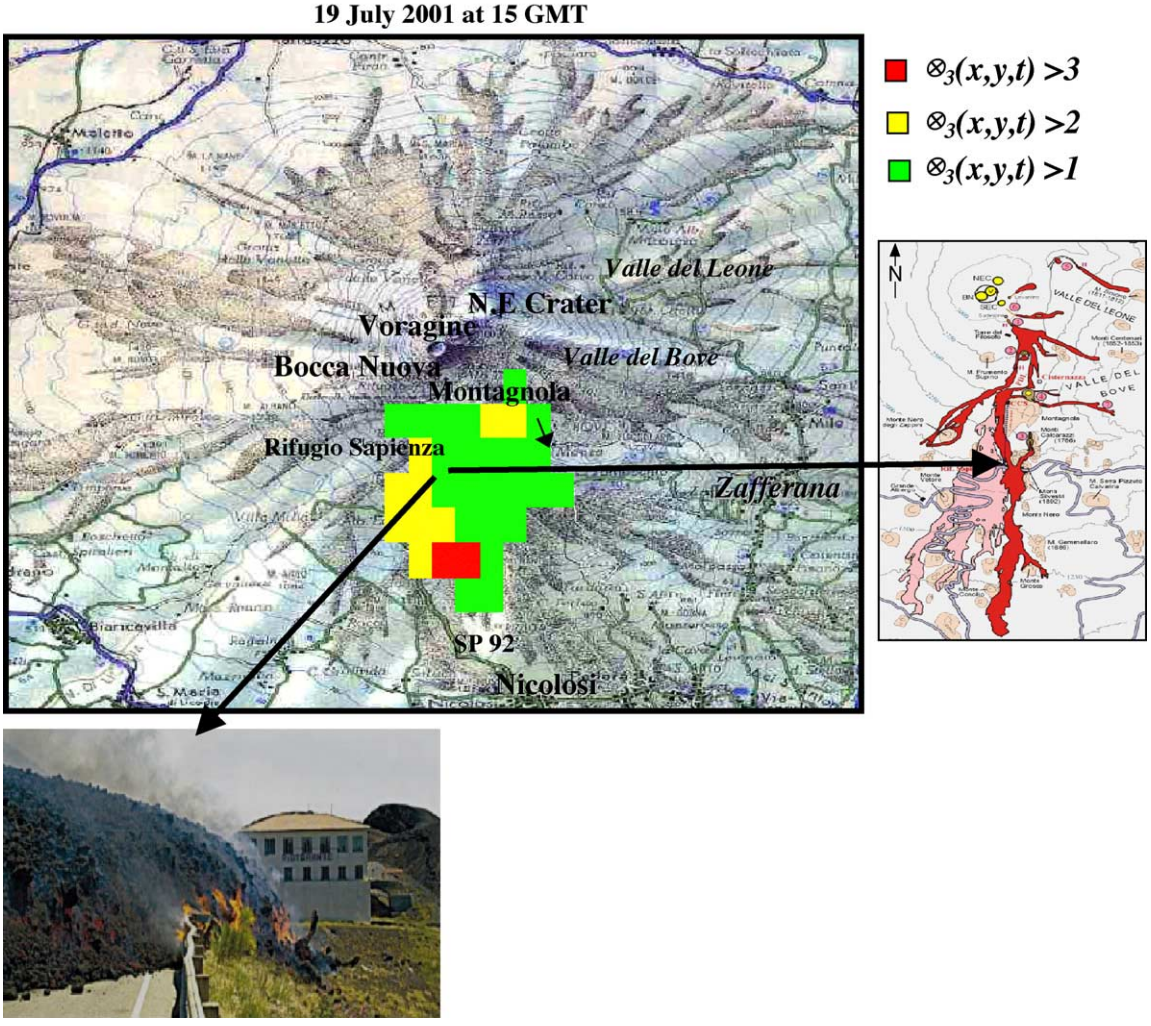

Fig. 6. RAT out comings obtained for July 19th have been colocated to a georeferenced map of Mount Etna. Different values of ALICE index are shown. Pixels with $\otimes_3(x,y,t)>3$ are depicted in red, pixels with $\otimes_3(x,y,t)>2$ and with $\otimes_3(x,y,t)>1$ are depicted in yellow and green, respectively. Lower values of ALICE index can be related to thermal anomalies of lower intensity or to small portion of lava flows within the pixel. Right side: map of the actual shape and location of lava flows and fissures. Bottom: a photograph documenting the lava crossing through the Provincial Road SP92.

accordance with the dynamic evolution of the events. Results obtained for the two most recent Etna eruptions (2001 and 2002) are shown, because documented and detailed maps of lava flows were available only for these events.

Concerning the eruption of July 2001, two maps are shown, the first one related to the beginning of the eruption, the second to the period of the peak of volcanic activities. In Fig. 6 the map derived for 19 July is reported. On this date, four new fissures were already active as a consequence of the flank activity that started on 17 July. All the detected thermal anomalies, shown in Fig. 6 with different colour codes according to anomaly intensities, are in accordance with the map of lava flows (produced by Istituto Nazionale di Geofisica e Vulcanologia, Sezione di Catania-INGV 2001) shown on the right side. In particular, a clear thermal anomaly was detected over Provincial Road SP92, according to the crossing of lava flow which occurred that day and that is documented in the photograph (Behncke, 2001) reported at the bottom of the same figure. It should be stressed once more that different values of $\otimes_3(x,y,t)$ can be associated with different thermal anomaly intensities. Lower values of the ALICE index could be related also to smaller portions of molten lava within the pixel of the satellite image.

In Fig. 7, results achieved on 24 July 2001 at 01GMT are shown. At that time, all the new fractures that had opened on the volcano's flank were active. Furthermore, two new eruptive activities started on 20 July at Levantino and in Valle del Leone (Behncke, 2001) and both were detected by the proposed technique. In fact, looking at Fig. 7 where, once more, thermal anomalies detected on the study area are shown (in red) together with the scheme of the lava flows, a new thermal anomaly (see the elongated shape anomaly in the upper part of the image) appears which was not present on the July 19th image shown before (Fig. 6). Moreover, the increase in volcanic activity, which occurred because of the opening of new fractures, has been recognised by RAT as well, as confirmed by the increased number of high-intensity anomalous pixels compared to the ones identified on 19 July, shown in Fig. 6. In conclusion, it seems that not only a precise mapping of the lava flows but also a detailed monitoring, in the space–time domain, of thermal anomalies is achievable by means of the proposed approach.

3.5. Pre-eruptive thermal anomaly detection

As mentioned before, the RAT intrinsic tuneability may allow us to investigate also for possible thermal anomalies of weaker intensity. Such signals might potentially be related to a low level thermal activity of volcanic unrest and, if detected before the beginning of the main eruptive events might be interpreted as signs of impending eruptions, even if a direct confirmation of this connection is still lacking. Anyway, in order to also confirm RAT capabilities in detecting such possible pre-eruptive anomalous thermal signals, satellite data series acquired before the beginning of the studied eruptive events were investigated as well.

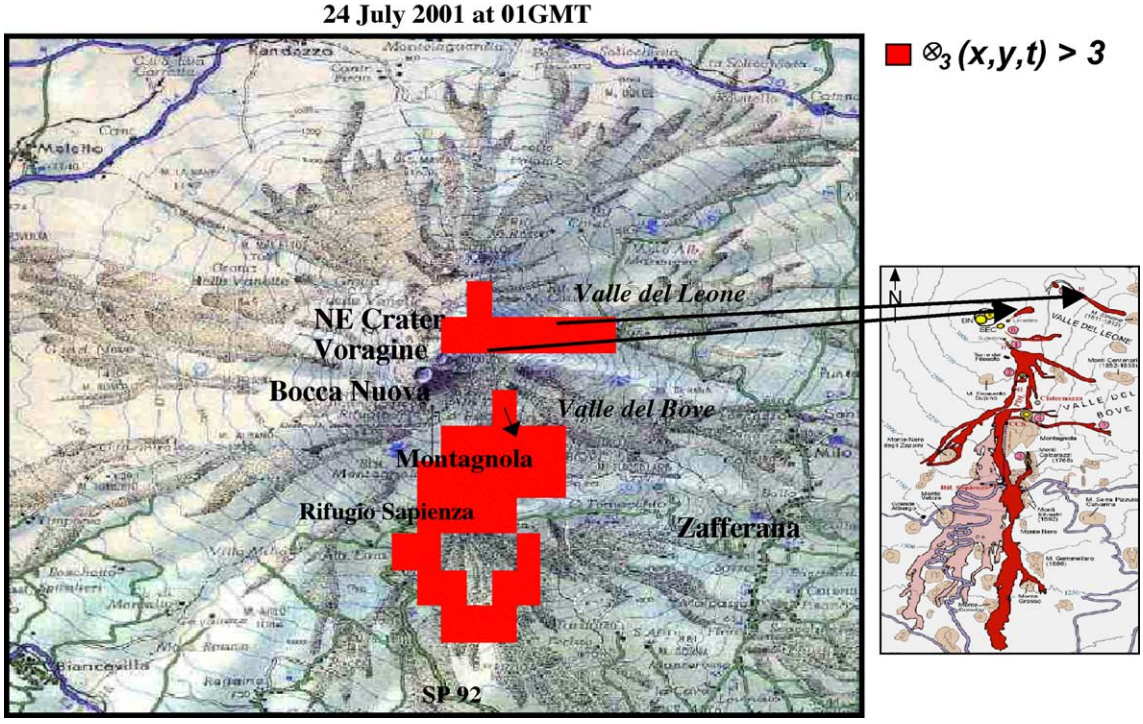

Fig. 7. RAT out comings obtained for July 24th have been colocated with a georeferenced map of Mount Etna. Pixels with $\otimes_3(x,y,t)>3$ are depicted in red. Right side: map of the actual shape and location of lava flows and fissures.

Several other authors have observed, for Mt. Etna and different volcanoes, a period of increase in thermal activity preceding the beginning of main eruptive events; pre-eruptive thermal anomalies were detected over summit areas (Dehn et al., 2002; Galindo & Dominguez, 2002), within lake waters (Sigurdsson, 1977; Vandemeulebrouck et al., 2000) and in wells and groundwaters (Badrudin, 1994; Bonfanti et al., 1996; Decker & Decker, 1981). Due to the very low thermal conductivity of volcanic rocks, such thermal changes are essentially produced by the escaping of very hot, magmatic gases through the cracks and the hydrothermal systems of volcanic edifices. Temperature variations may then occur which, however, are expected to be less intense than thermal anomalies detected during the phases of lava effusion. In this section, a further investigation has been carried out in order to determine whether pre-eruptive thermal anomalies (if any) can possibly be detected by the proposed approach. In Fig. 8, the situation observed on 13 July, few days before the beginning of the strong flank activity, is shown. On 13 July, a new intense paroxysm event occurred at the South East Crater while lava flowed from Levantino. Both these events were detected by the RAT technique as can be seen in Fig. 8 looking at the red and yellow areas representing, respectively, pixels with $\otimes_3(x,y,t)>3$ and $\otimes_3(x,y,t)>2$. Moreover, an isolated thermal anomaly with $\otimes_3(x,y,t)>2$ has been observed on the southern flank of the volcano. This anomaly, which cannot be related to the two aforementioned episodes, had appeared within an area ($\approx$2700 m elevation) where 4 days later a new eruptive fracture opened, throwing out lava flows. This fracture was one of the most active and its lava flows menaced Rifugio Sapienza, destroying part of the cable car. This analysis (as documented in Di Bello et al., in press) has been independently confirmed by direct ground observations (reporting a sudden and intense air warming at the same place and in the same day).

In order to investigate more in depth RAT capabilities and to better assess these preliminary results, a similar investigation has been carried out for the eruptive events of Etna and Stromboli which occurred in October–November 2002. In this further analysis, the higher sensitivity offered by AVHRR Thermal Infrared (TIR) band (centred around 11 μm) to emitting surfaces at lower temperature has also been exploited because, as mentioned before, possible thermal precursors should have lower intensities than magmatic sources. Similarly, the relevant ALICE index for the TIR band can be expressed as follows:

$$\otimes_4(x,y,t) = \frac{[T_4(x,y,t) - <T_4(x,y)>]}{\sigma_4(x,y)}$$

with an obvious meaning of symbols. As is well known, additional limitations should be taken into account dealing with these spectral records. For example, environmental effects (atmospheric and surface temperature fluctuations,

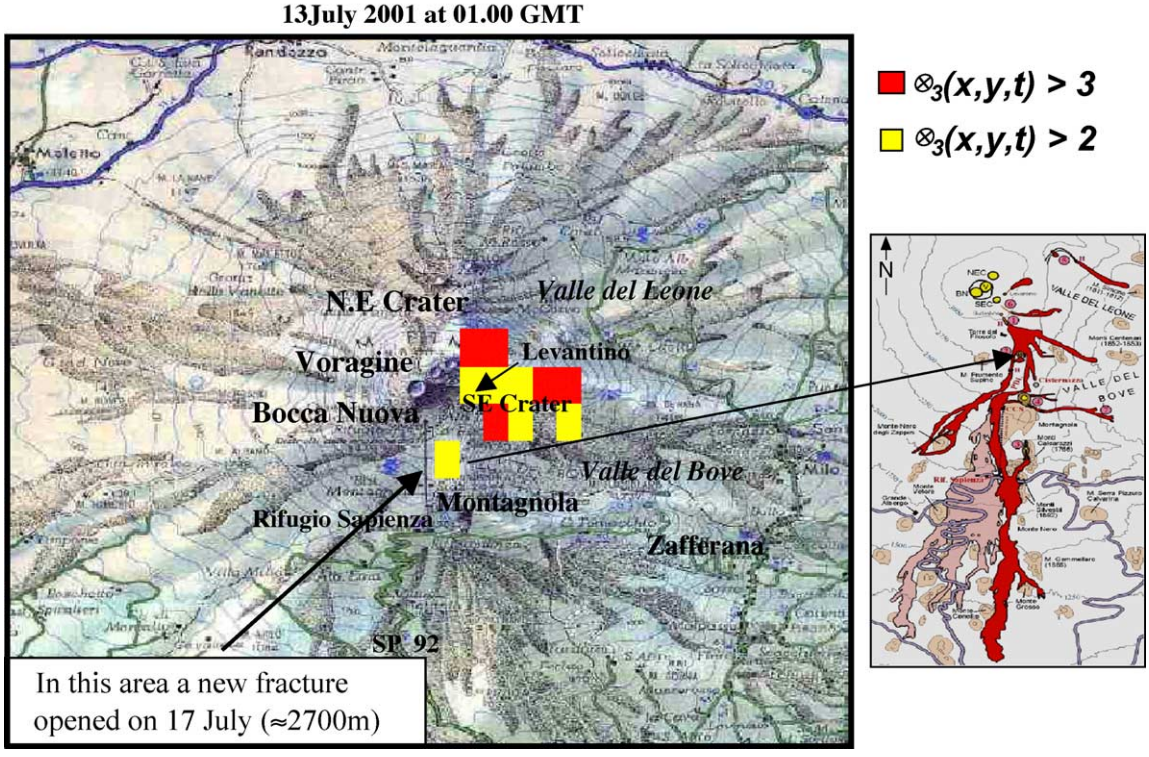

Fig. 8. RAT out comings obtained for July 13th have been colocated with a georeferenced map of Mount Etna. Different values of ALICE index are shown. Pixels with $\otimes_3(x,y,t)>3$ are depicted in red whereas all pixels where $\otimes_3(x,y,t)>2$ are yellow coloured. Right side: map of the actual shape and location of lava flows and fissures. An isolated thermal anomaly was detected by RAT, located within the area (~2700 m) where the four days later new fissure opened on the southern flank of volcano.

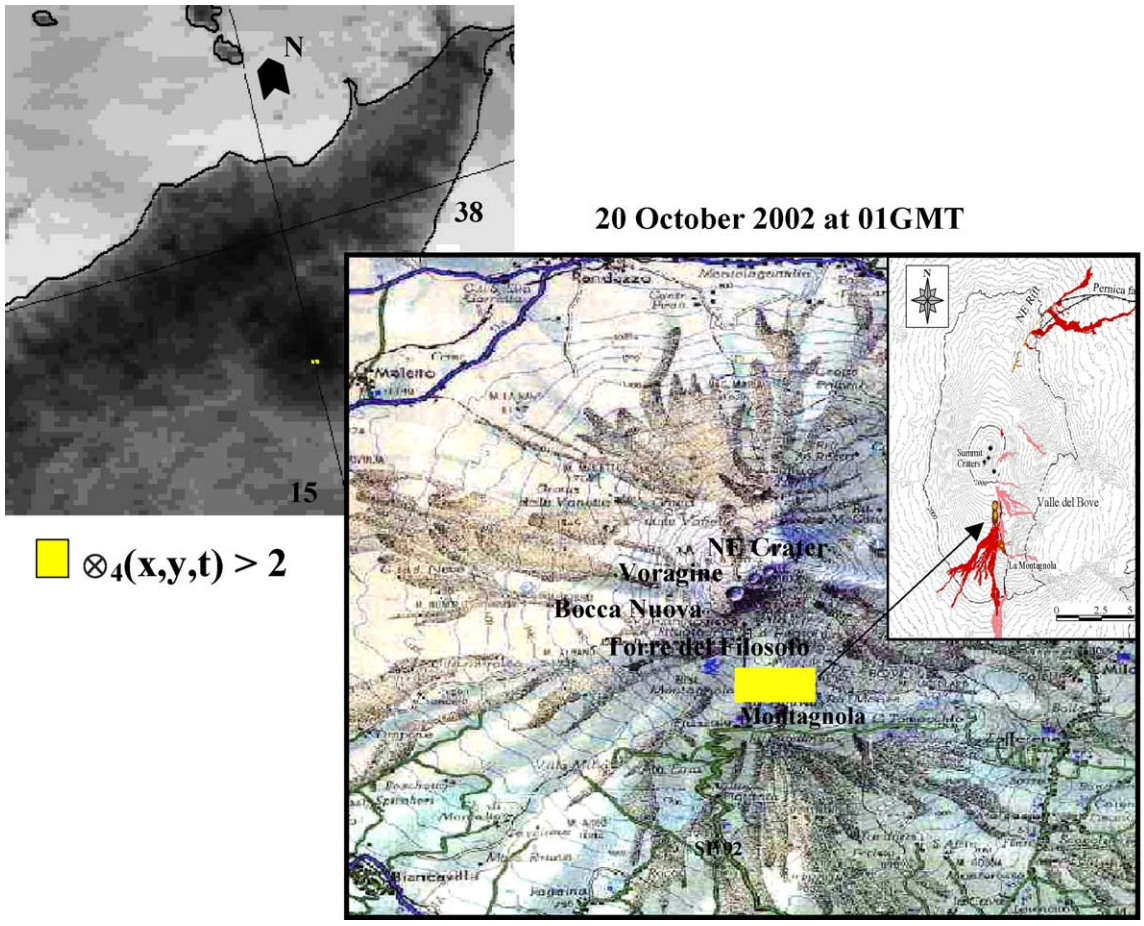

Fig. 9. RAT results obtained for 20 October 2002. Detected thermal anomalies are shown on a magnification of AVHRR pass around Etna area (top) and have been colocated with a georeferenced map of Mount Etna (bottom). ALICE index values $\otimes_4(x,y,t)>2$ (i.e., derived for AVHRR channel 4) are shown in yellow. Inset: Map of the actual shape and location of lava flows and new fissures. Thermal anomalies detected by RAT are located on and around the area where the new fissure opened on the southern flank of Etna volcano on 27 October 2002.

weather-related effects, etc.) may affect the TIR spectral region more than the MIR one. Nevertheless, as it will be shown afterwards, the information provided by this spectral band can be in some cases, and provided the proposed approach is applied, profitably used for low level thermal anomaly detection as well.

In Figs. 9 and 10, RAT results obtained processing AVHRR satellite data acquired in October 2002 are shown. All satellite products have been colocated to a georeferenced map of Mt. Etna and all the results have been compared with a map of actual lava flows produced by INGV (Ingv-Sezione di Catania, 2002).

In Fig. 9 the RAT satellite product obtained for channel 4 on 20 October is shown. As can be seen from the Figure, a thermal anomaly with $\otimes_4(x,y,t)>2$ located in the southern area of Mt. Etna was identified, while no other pixels were flagged elsewhere. The comparison with the map of lava flows, reported on the right side of the same figure highlights that the hotspot detected by RAT was located on and around the area where 7 days later the new southern fissure opened, on the flank of Etna volcano. It is as well to remember that AVHRR channel 4 is more sensitive to sources at lower temperatures than channel 3. Therefore, it can be supposed that the thermal anomaly detected by RAT was related to a magma rising or a hot gas emission, since no actual lava flows were present in this area at the time of data imaging. This may explain why the ALICE index in channel 4 [$\otimes_4(x,y,t)$] did reveal the anomalous signal, whereas the $\otimes_3(x,y,t)$ did not.

Similarly to Fig. 9, in Fig. 10, RAT results obtained for October 22nd are shown. A thermal anomaly of quite a high intensity [$\otimes_3(x,y,t)>3$] is detected exactly in the area where 5 days later the new northern fissure opened, as confirmed by looking at the map of fissures and lava flows reported in the same figure. In this case, the high value of the thermal anomaly suggests the presence of a near surface hot source (for example shallow magma) emitting a radiance peaking in the MIR AVHRR spectral band. Furthermore, looking at the bottom of the same figure, where two level thermally anomalous pixels are reported [in red and yellow for $\otimes_3(x,y,t)>3$ and $\otimes_3(x,y,t)>2$, respectively], the size and shape of the detected thermally anomalous areas, seem to be rightly related to the actual spatial distribution of the new fractures, as well.

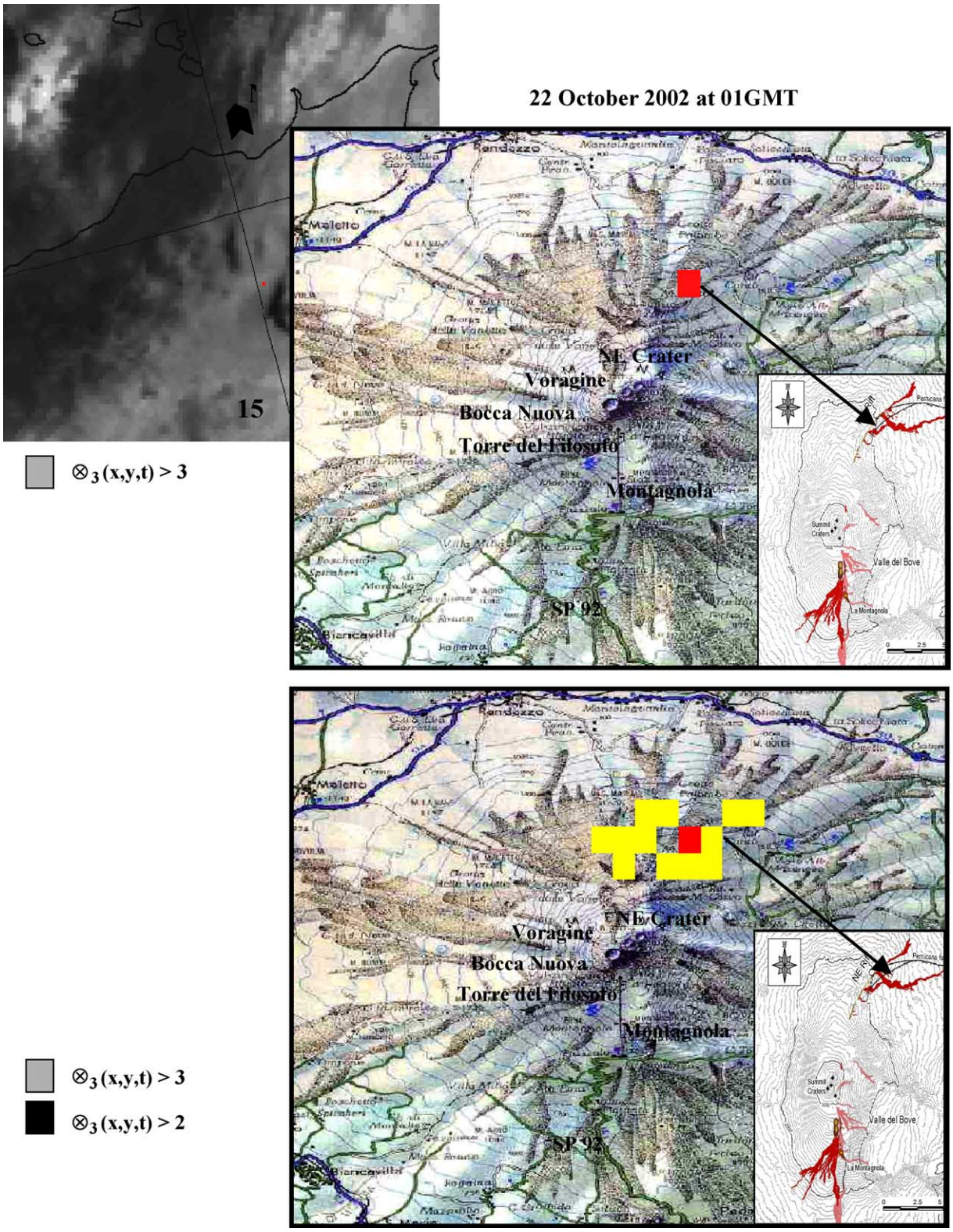

Fig. 10. RAT results obtained for 22 October 2002. Detected thermal anomalies are shown on a magnification of AVHRR pass around Mt. Etna (top) and have been colocated with a georeferenced map of Mount Etna (bottom). ALICE index values $\otimes_3(x,y,t)>2$ (yellow) and $\otimes_3(x,y,t)>3$ (red) are shown. Inset: Map of the actual shape and location of lava flows and new fissures. Location of detected thermal anomalies seem to be well correlated to the actual shape and size of lava flows as well as to the spatial distribution of the fractures opened on the northern flank of Etna volcano on 27 October.

These results show that anomalous thermal signals were detected by RAT some days before the beginning of Mt. Etna flank eruptions, in both the northern and southern area of Etna volcano exactly where the two new fissures opened on 27 October 2002. This fact appears to be even more important considering that the October–November 2002 Etna eruption was more dangerous and more devastating than the previous flank eruption, as it had very few precursors that did not permit in every case to foresee and predict this event (Behncke, 2002). By reading the reports (Smithsonian Institute, 2002), in fact, only at 10:25 PM of 26 October (i.e., a few hours before the beginning of the eruptive event) a swarm of earthquakes was detected and this was the only significant sign of the impending eruption.

Therefore, such preliminary results show that the proposed technique, considering both radiances in AVHRR channels 3 and 4, is not limited to detect hotspots with high reliability, but it might potentially be used to also identify signal transients of lower intensity which can possibly announce impending eruptions. It should also be stressed as such a capability is achieved by RAT without any deterioration in terms of false identification rate. Nevertheless, it has to be considered that new evidences should be retrieved in order to confirm such results and to better understand the physical nature of the observed thermal signals. A longer, temporal series of satellite images should be investigated for example, searching for possible similar signals also during no-eruptive periods, in order to better assess such results both in terms of robustness and reliability. Such an analysis, carried out over a temporal series of satellite subscenes acquired over the Etna volcano area during 1 year, is going ahead as a work in progress in order to verify the possible presence of false positive signals coming from the volcano itself during no-eruptive periods.

4. Discussion and conclusions

The application of the Robust AVHRR Techniques (RAT) approach to automatically detect volcanic thermal features related to eruptive activity has been addressed in this paper considering some recent eruptive events of Mt. Etna and Stromboli volcanoes. Preliminary results have confirmed that such a technique can be successfully used to detect and monitor thermal anomalies related to volcanic activity ensuring low false alarm rate and high detection sensitivity.

Several seasonal (e.g., summer/winter) and observational (e.g., night/day/afternoon) conditions have been considered, in order to assess RAT capabilities and limitations. The proposed approach showed a good reliability in very different observational conditions; it demonstrated to be not affected (as, instead, happens for techniques based on a differential approach) by the solar reflected component of radiation as well as by the natural warming of volcanic rocks, both generally producing "false positive" signals. These effects, in fact, occurred typically in the same places under the same observational conditions, so they are considered as the "normal state" by RAT technique that, consequently, doesn't produce false alarms. In all the considered study cases (Etna eruption of January–February 1999, July–August 2001 and October–November 2002 and the eruption which interested Stromboli volcano in November–December 2002) the proposed technique was able to automatically identify hotspots related to eruptive activities, as well as to monitor the space–time evolution of volcanic thermal features. A limited, residual number of false alarms (<1%) has been observed on the whole data set investigated. Because most of the false positives came from clouds over the area, an accurate cloud detection algorithm applied in preprocessing could further reduce the false alarm rate. An increasing of the false alarm rate could be observed at lower values of ALICE index which should be used when the observational conditions (i.e., daytime, summer season) reduce RAT sensitivity.

The spatial accuracy of the hotspot mapping has been validated also by colocating AVHRR products on a georeferenced map of the Mount Etna area. All the detected thermal anomalies were rightly located on the areas of Mt. Etna volcano affected by the eruptive episodes and all of them were in good accordance with the size and location of the actual lava flows. In terms of monitoring capabilities, the present technique seems to have confirmed its effectiveness. As an example, the increase of volcanic activity which occurred during the Mt. Etna eruptive events following 17 July 2001 was rightly recognised by RAT and figured out by analysing the evolution of the eruptive event in the space–time domain.

The analysis carried out on the recent Etna and Stromboli eruptions of 2002 has confirmed the technique performances and capabilities, suggesting its usefulness for near real-time monitoring of volcanic activity. Such an analysis has also confirmed the self-adaptability of RAT, since it was successfully applied under very different observational and natural conditions. The main limitations of the present approach are related to the cloud coverage, which over volcanoes could be a severe problem, and to the possible presence of burning fires over the investigated area, which might be erroneously interpreted as volcanic thermal anomalies. Actually, the difficulty induced by cloud coverage is a common problem for all techniques working with IR records, as clouds prevent the observation of the underlying surfaces (e.g., Tupper et al., 2004). The problem of bushfires still remains a serious one, as the signal produced by these two different events (fires and eruptive activity) is practically the same. However, the nearest areas to active volcanic craters are often unvegetated zones, with a low probability of fires occurrence.

Furthermore, the proposed approach has been applied in order to assess its potential in detecting lower levels of anomalous thermal signals, possibly related to preparedness phases of volcanic eruptions. The observation of pre-eruptive

thermal anomalies (revealed in both MIR and TIR infrared AVHRR channels and for several study cases) some days before the beginning of the main eruptive events, suggests that the RAT technique is also sensitive to anomalous signals of lower intensity, that may sometimes precede new eruptive events. This circumstance, if confirmed by further analyses on extended statistics of events and on different volcanoes, will allow us to use the RAT approach not only to automatically detect hotspots and monitor volcanic activity in near real-time but also to timely identify possible precursor signals of impending eruptive events.

The proposed technique, being only based on satellite records may be easily exported to whatever satellite sensors. In particular, significant improvements, essentially thanks to the expected reduction of the observational noise, can be achieved by the extension of the proposed approach to geostationary satellites like Meteosat Second Generation-Spinning Enhanced Visible and Infrared Imager (MSG-SEVIRI) offering a time resolution of 15 min and a channel selection which saves (and extends) present AVHRR capabilities.

Even at a lower spatial resolution (3 km compared with 1.1 km of AVHRR in the TIR channels) and thanks to the MSG geostationary attitude, SEVIRI will offer:

(a) an accurate geocorrection and a natural image-to-image colocation, as well as constant (for each location) view angles that permit a strong reduction of the observational noise and the increasing of sensitivity of RAT which strongly relies on the multitemporal analysis of satellite radiance on a pixel-by-pixel base.
(b) an improved time resolution that will reduce both the natural (lower image-to-image variability of the *llocal* signal) and observational (higher homogeneity of time series elements) noise increasing, again, the sensitivity of ALICE indices toward relatively lower signal variations.

Such capabilities are particularly important when a real-time monitoring as well as a deeper investigation on pre-eruptive signal identification is aimed at.

On the other hand, exploiting the Earth Observing System-Moderate Resolution Imaging Spectroradiometer (EOS-MODIS) capabilities (e.g., the better radiometric resolution, the higher dynamic range of the midinfrared band, the improved spectral channel selection) will make it possible to improve performances of the proposed approach especially for what concerns accuracy of lava flow mapping and precision in retrieving lava physical properties. Finally, if both opportunities will properly complement each other, a concrete contribution to the development of a satellite surveillance system can be achieved, to better monitor thermal features of active volcanoes and to possibly identify an integrated, global, observing strategy devoted to volcanic hazard mitigation.

References

Badrudin, M. (1994). Kelut Volcano monitoring: Hazards, mitigation and changes in water chemistry prior to the 1990 eruption. *Geochemical Journal*, *28*, 233–241.

Behncke, B. (1999). Etna Decade Volcano, Sicily, Italy—Updates January 1999, http://boris.vulcanoetna.com/ETNA_news.html.

Behncke, B. (2001). Etna Decade Volcano, Sicily, Italy—Updates July 2001. http://boris.vulcanoetna.com/ETNA_news.html.

Behncke, B. (2002). Etna Decade Volcano, Sicily, Italy—Updates October 2002. http://boris.vulcanoetna.com/ETNA_news.html.

Bonfanti, P., D'Alessandro, W., Dongarra, G., Parello, F., & Valenza, M. (1996). Medium-term anomalies in groundwater temperature before 1991–1993 Mt. Etna eruption. *Journal of Volcanology and Geothermal Research*, *73*, 303–308.

Carn, S. A., & Oppenheimer, C. (2000). Remote monitoring of Indonesian volcanoes using satellite data from the Internet. *International Journal of Remote Sensing*, *21*(5), 873–910.

Cuomo, V., Lasaponara, R., & Tramutoli, V. (2001). Evaluation of a new satellite-based method for forest fire detection. *International Journal of Remote Sensing*, *22*(9), 1799–1826.

Dean, K. G., Servilla, M., Roach, A., Foster, B., & Engle, K. (1998). Satellite monitoring of remote volcanoes improves study efforts in Alaska. *EOS Transaction American Geophysical Union*, *79*(413), 422–423.

Decker, R., & Decker, B. (1981). *Volcanoes*. San Francisco, CA: Freeman.

Dehn, J., Dean, K. G., & Engle, K. (2000). Thermal monitoring of North Pacific volcanoes from space. *Geology*, *28*(8), 755–758.

Dehn, J., Dean, K. G., Engle, K., & Izbekov, P. (2002). Thermal precursors in satellite images of the 1999 eruption of Shishaldin Volcano. *Bulletin Volcanologique*, *64*, 525–534.

Di Bello, G., Filizzola, C., Lacava, T., Marchese, F., Pergola, N., Pietrapertosa, C., et al. (2004). Robust satellite techniques for volcanic and seismic hazards monitoring. *Annals of Geophysics*, *47*(1) (in press).

Dozier, J. (1981). A method for satellite identification of surface temperature fields of subpixel resolution. *Remote Sensing of Environment*, *11*, 221–229.

Flynn, L. P., Wright, R., Garbeil, H., Harris, A. J. L., & Pilger, E. (2002). A global thermal alert using MODIS: Initial results from 2000–2001. *Advances in Environmental Monitoring and Modelling*, *1*, 5–36.

Galindo, I., & Dominguez, T. (2002). Near real-time satellite monitoring during the 1997–2000 activity of Volcan de Colima (Mexico) and its relationship with seismic monitoring. *Journal of Volcanology and Geothermal Research*, *117*, 91–104.

Gaonac'h, H., & Vandemeulebrouck, P. J. (1994). Thermal infrared satellite measurements of volcanic activity at Stromboli and Vulcano. *Journal of Geophysical Research*, *99*, 9477–9485.

Gawarecki, S. J., Lyon, R. J. P., & Nordberg, W. (1965). Infrared spectral returns and imagery of the Earth from space and their application to geological problems. *Science and Technological Series—American Astronomical Society*, *4*, 13–33.

Harris, A. J., Pilger, E., & Flynn, L. P. (2002). Web-based hot spot monitoring using GOES: What it is and how it works. *Advances in Environmental Monitoring and Modelling*, *1*(3), 5–36.

Harris, A. J., Pilger, E., Flynn, L. P., Garbeil, H., Mouginis-Mark, P. J., Kauahikaua, J., et al. (2001). Automated high temporal resolution thermal analysis of Kilauea volcano, Hawai'i, Using GOES satellite data. *International Journal of Remote Sensing*, *22*(6), 945–967.

Harris, A. J., Swabey, S. E. J., & Higgins, J. (1995). Automated threshold of active lava using AVHRR data. *International Journal of Remote Sensing*, *16*(18), 3681–3686.

Harris, A. J., Vaughan, R. A., & Rothery, D. A. (1995). Volcano detection and monitoring using AVHRR data: The Krafla eruption, 1984. *International Journal of Remote Sensing*, *16*, 1001–1020.

Harris, A. J., Wright, R., & Flynn, L. P. (1999). Remote monitoring of Mount Erebus volcano, Antarctica, using polar orbiters: Progress and

prospect. *International Journal of Remote sensing*, *20*(15 and 16), 3051–3071.

Higgins, J., & Harris, A. J. L. (1997). Vast: A program to locate and analyse volcanic thermal anomalies automatically from remotely sensed data. *Computers and Geosciences*, *23*(6), 627–645.

Ingv-Research Staff Sezione di Catania (2001). Multidisciplinary approach yields insight into Mt. Etna eruption. *EOS Transaction American Geophysical Union*, *82*(52), 653–656.

Ingv-Sezione di Catania (2002). Osservatorio sull'eruzione Stromboli 2002, web site: http://www.ct.ingv.it/Stromboli2002/Main.htm.

Kidwell, K. (1991). NOAA Polar Orbiter Data User's Guide. NCDC/SDSD. National Climatic Data Center, Washington, DC.

Lacava, T., Di Leo, E. V., Pergola, N., Romano, F., Sannazzaro, F., & Tramutoli, V. (2004). Analysis of multi-temporal satellite records for extreme flooding events monitoring. Mediterranean storms—Proceedings of the 3rd EGS Plinius Conference held at Ajaccio, Corsica, France, October 2003 @ 2003 by Editrice (in press).

Lasaponara, R., Cuomo, V., & Tramutoli, V. (1998). Fire detection by AVHRR: Toward a new approach for operational monitoring. In Edwin T. Engman (Ed.), *Proceedings of SPIE*. *Remote Sensing for Agriculture, Ecosystems and Hydrology*, *vol. 3499* (pp. 348–355).

Marchese, F. (2001). Tecniche satellitari avanzate per il monitoraggio dell'attività vulcanica nell'infrarosso termico. Degree Thesis available at the University of Basilicata, Potenza, Italy.

Oppenheimer, C. (1998). Volcanological applications of meteorological satellites. *International Journal of Remote Sensing*, *19*(15), 2829–2864.

Pergola, N., Pietrapertosa, C., Lacava, T., & Tramutoli, V. (2001). Robust satellite techniques for volcanic eruptions monitoring. *Annals of Geophysics*, *44*(2), 167–177.

Pergola, N., Pietrapertosa, C., & Tramutoli, V. (1998). Satellite remote sensing of volcanic aerosols: A new, AVHRR-based, approach. In Jacqueline E. Russel (Ed.), *Proceedings of SPIE*. *Satellite remote sensing of clouds and the Atmosphere III*, *vol. 3495* (pp. 188–197).

Pergola, N., & Tramutoli, V. (2000). SANA: Sub-pixel Automatic Navigation of AVHRR imagery. *International Journal of Remote Sensing*, *21*(12), 2519–2524.

Pergola, N., & Tramutoli, V. (2003). Two years of operational use of SANA (Sub-pixel Automatic Navigation of AVHRR) scheme: Accuracy assessment and validation. *Remote Sensing of Environment*, *82*(2), 190–203.

Pergola, N., Tramutoli, V., Scaffidi, I., Lacava, T., & Marchese, F. (2004). Improving volcanic ash clouds detection by a robust satellite technique. *Remote Sensing of Environment*, *90*(1), 1–22.

Prata, A. J. (1989). Observations of volcanic ash clouds in the 10–12 μm window using AVHRR/2 data. *International Journal of Remote Sensing*, *10*, 751–761.

Rothery, D. A., Francis, P., & Wood, W. (1988). Volcano monitoring using short wavelength infrared data from satellite. *Journal of Geophysical Research*, *93*, 7993–8008.

Schneider, D. J., & Rose, W. I. (1994). Observations of the 1989–1990 Redoubt Volcano eruption clouds using AVHRR satellite imagery. In T. Casadevall (Ed.), *Proceedings of the First International Symposium on Volcanic Ash and Aviation Safety. U.S. Geological Survey Bulletin*, *vol. 2047* (pp. 405–418).

Schneider, D. J., Rose, W. I., & Kelley, L. (1995). Tracking of 1992 eruption clouds from Crater Peak of Mount Spurr Volcano, Alaska, using AVHRR. *U.S. Geological Survey Bullettin*, *2139*, 27–36.

Smithsonian Institute (2002). Global Volcanism Program—Volcanic Activity Reports, http://www.volcano.si.edu/gvp/.

Sigurdsson, H. (1977). Chemistry of the crater lake during the 1971–72 Soufrière eruption. *Journal of Volcanology and Geothermal Research*, *2*, 165–186.

Tramutoli, V. (1998). Robust AVHRR Techniques (RAT) for Environmental Monitoring theory and applications. In Giovanna Cecchi, & Eugenio Zilioli (Eds.), *In Earth Surface Remote Sensing II*. *SPIE*, *vol. 3496* (pp. 101–113).

Tramutoli, V., Di Bello, G., Pergola, N., & Piscitelli, S. (2001a). Robust satellite techniques for remote sensing of seismically active areas. *Annals of Geophysics*, *44*(2), 295–312.

Tramutoli, V., Pergola, N., & Pietrapertosa, C. (2001b). Training on NOAA-AVHRR of robust satellite techniques for next generation of weather satellites: An application to the study of space–time evolution of Pinatubo's stratospheric volcanic cloud over Europe. In W. L. Smith, & Yu. M. Timofeyev (Eds.), *IRS 2000: Current problems in atmospheric radiation* (pp. 36–39). Hampton, VA: A. Deepak Publishing.

Tupper, A., Carn, S., Davey, J., Kamada, Y., Potts, R., Prata, F., et al. (2004). An evaluation of volcanic cloud detection techniques during recent significant eruptions in the western 'Ring of Fire'. *Remote Sensing of Environment*, *91*, 27–46.

Vandemeulebrouck, J., Sabroux, J. C., Halbwachs, M., Poussielgue, N., Grangeon, J., & Tabbagh, J. (2000). Hydroacoustic noise precursors of the 1990 eruption of Kelut Volcano, Indonesia. *Journal of Volcanology and Geothermal Research*, *97*, 443–456.

Wright, R., Flynn, L., Garbeil, H., Harris, A., & Pilger, E. (2002). Automated volcanic eruption detection using MODIS. *Remote Sensing of Environment*, *82*, 135–155.

Wright, R., Flynn, L., Garbeil, H., Harris, A., & Pilger, E. (2004). MODVOLC: Near-real-time thermal monitoring of global volcanism. *Journal of Volcanological and Geothermal Research*, *135*(1–2), 29–49.